JOURNAL OF GEOPHYSICAL RESEARCH, VOL. 109, C12016, doi:10.1029/2003JC002086, 2004

An eddy viscosity formulation for oscillatory flow over vortex ripples

J. Malarkey and A. G. Davies

School of Ocean Sciences, University of Wales Bangor, Anglesey, UK

Received 7 August 2003; revised 6 September 2004; accepted 28 September 2004; published 14 December 2004.

[1] In two-dimensional oscillatory flow above steep ripples, momentum transfer in the near-bed layer is dominated by the process of vortex formation and shedding. Here results from a cloud-in-cell (CIC) discrete-vortex model representing this phenomenon are horizontally averaged and then used to infer the behavior of a one-dimensional vertical (1DV) "convective eddy viscosity." For symmetric waves, this eddy viscosity has a mean value that is consistent with empirically derived formulae based on laboratory measurements, and a second harmonic that decreases in amplitude from 3 times that of the mean value down to the size of the mean, as the ratio of orbital excursion amplitude to ripple wavelength increases. The peak value of this strongly time-varying eddy viscosity occurs at about the time of flow reversal in the free-stream, revealing the qualitatively different nature of the momentum transfer above rippled and flat beds. The general behavior of the eddy viscosity is explored, for ripples of different shape and steepness, through the vortex parameter range, and rules are proposed that allow the behavior of the new eddy viscosity to be extrapolated beyond this range toward the classical flat rough-bed limit. The simple, 1DV, convective eddy viscosity derived here may be used to represent the vortex-shedding process in large-scale practical formulations, and should lead to an improved representation of sediment transport in the rippled-bed regime. *INDEX TERMS:* 4211 Oceanography: General: Benthic boundary layers; 4255 Oceanography: General: Numerical modeling; 4546 Oceanography: Physical: Nearshore processes; 4560 Oceanography: Physical: Surface waves and tides (1255); *KEYWORDS:* eddy viscosity, oscillatory flow, vortex ripples

Citation: Malarkey, J., and A. G. Davies (2004), An eddy viscosity formulation for oscillatory flow over vortex ripples, *J. Geophys. Res.*, *109*, C12016, doi:10.1029/2003JC002086.

1. Introduction

[2] Vortex ripples that form on sandy beds in response to the oscillatory motion induced by surface waves are common features in coastal areas and shallow continental shelf seas. The near-bed hydrodynamics are completely dominated by the vortices shed from the steep ripple profiles, resulting in flow behavior that is qualitatively different from that above a flat bed. The vortex-shedding regime is delineated approximately by $0.5 \leq A_0/\lambda \leq 2$ and $0.13 \leq \eta/\lambda \leq 0.2$, where A_0 is the near-bed orbital excursion amplitude, and λ and η are the ripple wavelength and height, respectively. While the vortex-shedding process has been extensively modeled and measured in the two-dimensional horizontal-vertical plane [see, e.g., *Sato et al.*, 1984, *Lewis et al.*, 1995 and *Fredsøe et al.*, 1999], little emphasis has been placed to date on the development of simplified, one-dimensional formulations that may be used in practical applications, for example, larger coastal scale models. For their part, one-dimensional models have taken little account of rippled-bed effects, other than by inclusion of a ripple-enhanced equivalent bed roughness k_s (typically $k_s = 4\eta$ [*Fredsøe et al.*, 1999]) within an otherwise flat-bed modeling scheme, which necessarily fails to represent the fundamentally different processes occurring above vortex ripples. *Sleath* [1991], *Nielsen* [1992], and *Ranasoma and Sleath* [1992] inferred from measurements a mean eddy viscosity for very rough and rippled beds that is height invariant, and thereby markedly different from the usual linearly increasing eddy viscosity used above flat beds [see, e.g., *Trowbridge and Madsen*, 1984]. Nielsen and Sleath pointed out that in the near-bed layer in oscillating flow above large roughness elements or steep ripples, momentum transfer is dominated by the vortex-shedding process rather than by random turbulence.

[3] In order to help bridge this gap, *Davies and Villaret* [1997] developed the concept of a "convective eddy viscosity," based on two-dimensional intrawave measurements, and also model results, for symmetric waves. After having taken horizontal (ripple) averages of the respective results, they showed that the vortex-shedding process could be interpreted in terms of a "convective" stress, and hence represented by a strongly time-varying, height-invariant, eddy viscosity. *Davies and Villaret* [1997] showed that based on this picture, the classical forward Eulerian drift predicted by *Longuet-Higgins* [1953] at the edge of the boundary layer beneath (symmetric) progressive waves was reduced in the presence of ripples. *Davies and Villaret* [1999] went on to investigate the observed reversal in

0148-0227/04/2003JC002086$09.00

Eulerian drift at the edge of the boundary layer beneath weakly asymmetric progressive waves, this being an effect with potentially important consequences for net sediment transport and grain size sorting. They also suggested how the convective eddy viscosity might behave as a result of wave asymmetry over the full range of conditions of practical importance. More recently, *Davies and Thorne* [2002] have shown how a near-bed, convective eddy viscosity submodel can be interfaced with a traditional 1DV flat-bed Reynolds-averaged sediment transport model.

[4] The purpose of this paper is to test the convective eddy viscosity approach over a more complete range of symmetric-wave conditions in the vortex-ripple regime than investigated by *Davies and Villaret* [1997]. The model used for this purpose is a cloud-in-cell discrete vortex (CIC) model, which has been used to represent successfully the process of vortex shedding in oscillatory flow above ripples [see, e.g., *Perrier et al.*, 1995; *Malarkey and Davies*, 2002]. *Malarkey and Davies* [2002] showed that as A_0/λ increases, the CIC model is able to represent the first stages of the breakdown of coherent vortices into the more horizontally homogeneous turbulence that is expected under flat-bed conditions, both by comparisons with the two-dimensional experimental data of *Earnshaw* [1996] and also by examination of the behavior of the form drag on the ripple.

[5] In section 2 a brief description of the discrete vortex model and solution domain is given, along with some two-dimensional results. In section 3 the concept of a convective eddy viscosity is introduced for symmetric wave oscillations, together with a method for its determination, with particular reference to the data of *Ranasoma* [1992]. The model results are then compared with Ranasoma's data before the more general dependence of the convective eddy viscosity on A_0/λ and η/λ is considered. In sections 4 and 5, the discussion and conclusions are presented.

2. CIC Model Description and 2-D Model Results

[6] Discrete vortex models, such as the present and *Perrier et al.* [1995] CIC models, constitute the simplest and most direct way to represent vorticity transport (see review of *Sarpkaya* [1989]). In situations where there are sharp gradients in vorticity, discrete vortex models are better suited than Reynolds-averaged models, because they do not suffer from numerical diffusion associated with advection, and vortices can be concentrated where there is most vorticity. They do not require any turbulence closure assumptions and consequently do not produce any Reynolds-averaged turbulent quantities.

[7] The present CIC model [see *Malarkey and Davies*, 2002] seeks to solve the vorticity transport equation above one ripple by representing the vorticity field as a sum of discrete point vortices. The model uses the operator splitting method of *Chorin* [1973] whereby vortices are alternately diffused (by applying a random-walk jump to their position) and advected. The advection velocity is calculated on a grid using the cloud-in-cell method of *Christiansen* [1973]. All flow quantities are assumed to be periodic in the ripple wavelength (i.e., at $x = \pm\lambda/2$), and the boundary conditions on the velocity are that it tends to the free-stream value far away from the ripple surface and also that there is no slip on the ripple surface. In order to maintain the no-slip condition,

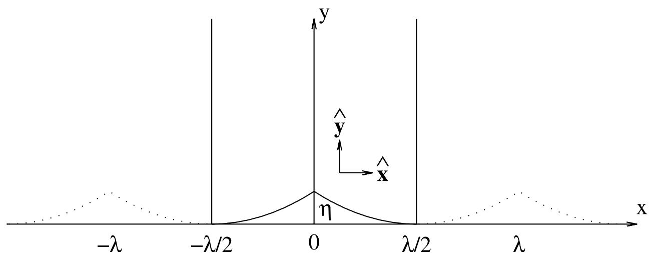

Figure 1. Definition sketch of the modeling domain for sharp-crested ripples (equation (1)).

new vortices are continually created along the ripple surface at each model time step. Because of the random-walk element, the final converged solutions considered later have been obtained by phase ensembling over a number (usually about 30) of wave periods. A more complete description of the model has been given by *Malarkey and Davies* [2002].

[8] Figure 1 shows a definition sketch of the solution domain for the CIC model, wherein λ is the ripple wavelength, η is the ripple height, and x and $\hat{\mathbf{x}}$ and y and $\hat{\mathbf{y}}$ are the horizontal and vertical co-ordinates and unit vectors, respectively. Thus the phase-ensembled velocity $\mathbf{u}$ is given by $u\hat{\mathbf{x}} + v\hat{\mathbf{y}}$, where u and v are the horizontal and vertical components of the velocity. In the case of Figure 1, the ripple is sharp-crested and given by

$$y = \eta\left(1 - \frac{2}{\lambda}|x|\right)^2, \quad |x| \le \frac{\lambda}{2}. \tag{1}$$

However, the present model makes use of a general mapping function which allows any realistic ripple, such as the round-crested ripple shape of *Ranasoma* [1992] shown in Figure 2, to be represented. A description of this mapping function together with the procedure for fitting it to a particular ripple shape has been given by *Malarkey* [2001].

[9] Figure 2 shows the vorticity ω ($= \partial v/\partial x - \partial u/\partial y$) from the CIC model in response to a symmetric, spatially uniform, horizontal, free-stream oscillation, used here and elsewhere, given by

$$u_\infty = U_0 \cos \sigma t, \tag{2}$$

where U_0 is the free-stream velocity amplitude, σ is the wave angular frequency ($= 2\pi/T$), T is the wave period, and t is the time. In the example shown, the wave orbital amplitude A_0 ($= U_0/\sigma$) is based on the parameter settings of *Ranasoma*'s [1992] test 2a. *Malarkey* [2001] showed that these contours agree quite well with the results from Ranasoma's experiment and also with equivalent results from *Perrier et al.*'s [1995] CIC model. Here the ejected vortex, E, formed in the previous half cycle begins to move off as the flow reverses at −90°. Also visible is the very weak relict vortex, R, from the previous wave half cycle. By −45° a growing vortex, G, is clearly visible on the (now) lee-side of the ripple; this continues to grow until the flow reverses at 90°. Meanwhile the ejected vortex loses strength (see phases 0° and 45°) until it, too, becomes insignificant. Once ejected, the vortex moves a distance approximately equal to $2A_0$, corresponding to the expected free-stream

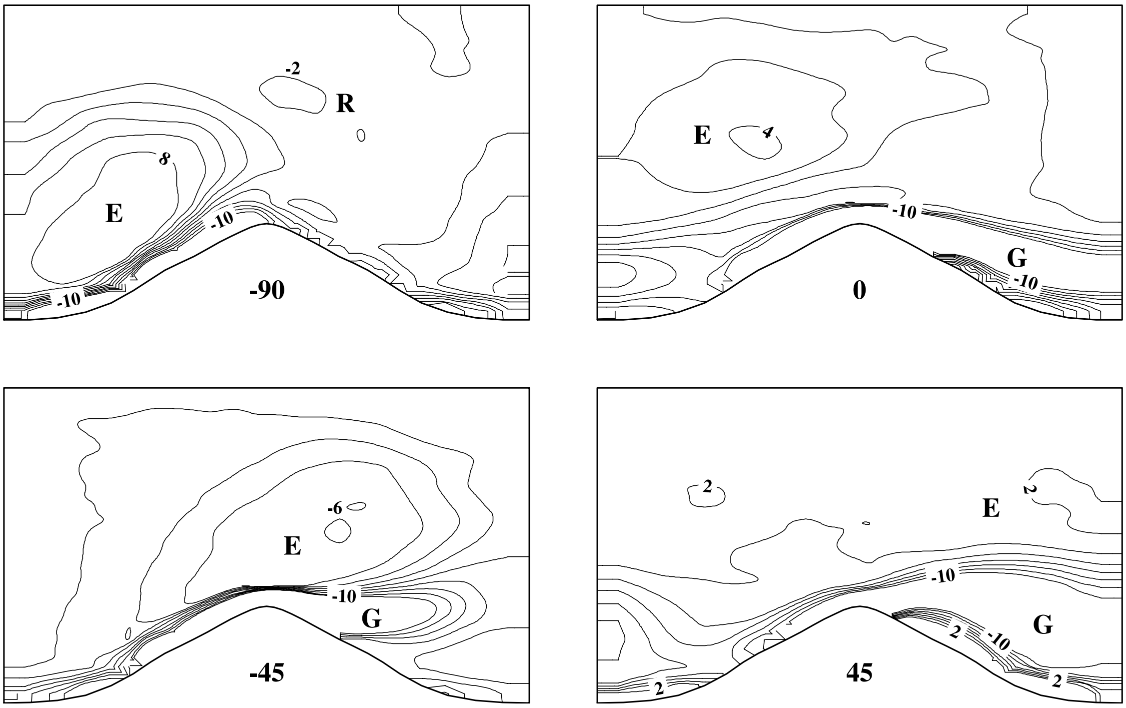

Figure 2. Nondimensional vorticity contours, $\omega\lambda/U_0$, (anticlockwise is positive, spacing = 2) from the present model in response to an oscillating free-stream velocity given by equation (2), for *Ranasoma*'s [1992] test 2a where $A_0/\lambda = 0.78$, $T = 2.41$ s, $\eta/\lambda = 0.184$ and $\lambda = 10$ cm, for various phases (degrees). E denotes a newly ejected vortex, G denotes the growing vortex on the lee side of the ripple, and R denotes the relict vortex from the previous wave half cycle.

advection during one wave half cycle. The flow then reverses and the process repeats itself, as described in more detail by *Malarkey and Davies* [2002]. All phase instants show that the vorticity is largely contained within the vertical region depicted, i.e., two ripple heights from the crest, and this region is termed the convective layer.

3. Convective Eddy Viscosity

3.1. Introduction

[10] The two-dimensional, Reynolds-averaged momentum equation, ignoring the viscous term, can be expressed as

$$\frac{\partial \mathbf{u}}{\partial t} + \mathbf{u}.\nabla\mathbf{u} = -\frac{1}{\rho}\nabla p + \mathbf{R}, \tag{3}$$

where $\nabla = \hat{\mathbf{x}}\,\partial/\partial x + \hat{\mathbf{y}}\,\partial/\partial y$, p is the nonhydrostatic pressure, ρ is the density, and $\mathbf{R}$ is the Reynolds stress term given by $[\partial\tau_{xx}/\partial x + \partial\tau_{xy}/\partial y]\,\hat{\mathbf{x}} + [\partial\tau_{yx}/\partial x + \partial\tau_{yy}/\partial y]\,\hat{\mathbf{y}}$ (where $\tau_{xx} = -(u'^2)_p$, $\tau_{xy} = \tau_{yx} = -(u'v')_p$, $\tau_{yy} = -(v'^2)_p$, u' and v' are the horizontal and vertical turbulent fluctuations in velocity, and $()_p$ represents a phase ensemble over a representative number of wave cycles). Now subject to the constraint that the flow is periodic over a ripple, and the assumption that the flow is incompressible ($\nabla.\mathbf{u} = 0$), the ripple-averaged horizontal component of equation (3) is given by

$$\frac{\partial\langle u\rangle}{\partial t} = -\frac{1}{\rho}\left\langle\frac{\partial p}{\partial x}\right\rangle + \frac{\partial\langle\tau_c\rangle}{\partial y}, \tag{4}$$

where $\langle\rangle$ represents the horizontal (ripple) average and $\langle\tau_c\rangle = -\langle uv\rangle - \langle(u'v')_p\rangle$. Here, since the advective term is included in $\langle\tau_c\rangle$ and the free-steam velocity is spatially uniform (see equation (2)), it follows that $\langle\tau_c\rangle = 0$ as $y \to \infty$ and, from the boundary layer approximation, that $\langle\partial p/\partial x\rangle = -\rho\partial u_\infty/\partial t$. By analogy with the gradient diffusion assumption, *Davies and Villaret* [1997] suggested that $\langle\tau_c\rangle$ could be represented by a convective eddy viscosity ν_{tc} defined with respect to the gradient of the horizontally averaged velocity, such that $\langle\tau_c\rangle = \nu_{tc}\partial\langle u\rangle/\partial y$.

[11] Equation (4) for the rippled-bed case can be compared with the equivalent, one-dimensional (1DV), flat-bed equation in which there are no appreciable advective terms,

$$\frac{\partial u}{\partial t} = \frac{\partial u_\infty}{\partial t} + \frac{\partial\tau_{xy}}{\partial y}. \tag{5}$$

However the solutions arising from equations (4) and (5) for oscillatory flow above rippled and flat beds, respectively, are strikingly different. This can be illustrated by comparing the two main quantities of interest: the horizontally averaged velocity, $\langle u\rangle$, and convective shear stress, $-\langle uv\rangle$, above ripples, with their flat-bed equivalents, u and $-(u'v')_p$, respectively. A comparison between the present CIC model results for $\langle u\rangle$ and $-\langle uv\rangle$ and results for u and $-(u'v')_p$ from a flat-bed, 1DV k-ε model [see *Malarkey et al.*, 2003] is presented in Figure 3. The two cases depicted correspond to the same Reynolds numbers, Re, ($Re = U_0A_0/\nu$, where ν is the kinematic viscosity) but different bed configurations ($k_s = 4\eta$, for the rippled bed [*Fredsøe et al.*, 1999], and $k_s = 2.5d$ where d is the grain diameter, for the flat rough bed) and different relative roughnesses, A_0/k_s. However, they allow a useful qualitative comparison. In the rippled-bed

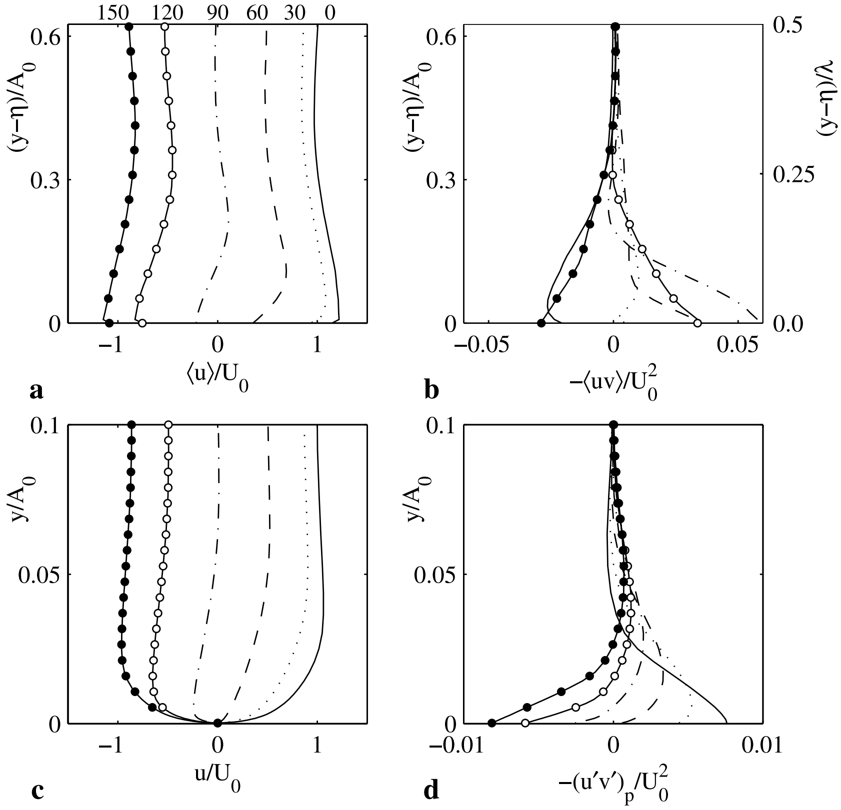

Figure 3. Vertical profiles, for various phase instants (given in Figure 3a in degrees) during the wave cycle of (a) $\langle u \rangle$ and (b) $-\langle uv \rangle$ over a sharp-crested ripple from the present CIC model, with $A_0/k_s = 1.25$ ($\eta/\lambda = 0.16$ and $A_0/\lambda = 0.8$), and (c) u and (d) $-(u'v')_p$ over a flat rough bed from a 1DV, k-ε model, with $A_0/k_s = 180$. (In both cases, $Re = 2.3 \times 10^4$, $A_0 = 17.6$ cm and $T = 8.46$ s.)

case, the horizontal averaging is only taken down to the crest level ($y = \eta$) below which $-\langle uv \rangle$ is increasingly replaced by form drag. In the flat rough-bed case this distinction is not explicit in the model solution, in which form drag is included but only occurs very close to the bed. To allow direct comparisons between the models, the vertical axes in Figure 3 are all scaled by the wave amplitude (A_0). A_0 is commonly used as a length scale for flat beds because the roughness elements are comparatively small. However, the more usual length scale to use for rippled beds, and that which is used in the rest of the paper, is the ripple wavelength (λ); therefore a secondary vertical axis scaled by λ is also included in Figure 3b.

[12] It can be seen that while the behavior of $\langle u \rangle$ and u, and $-\langle uv \rangle$ and $-(u'v')_p$, is broadly similar, there are also some marked differences. In both cases an overshoot in the velocity occurs (when $0 < (y - \eta)/A_0 < 0.13$, in the rippled-bed case, and $0.02 < y/A_0 < 0.06$, in the flat-bed case). This is the result of the gradient of the stress having a different phase relationship with height in respect of the acceleration term, such that in a certain height range the peak velocity becomes larger than that in the free-stream flow. The overshoot is much larger in the rippled-bed case (20% of U_0) than in the flat-bed case (6% of U_0). Also, the boundary layer is much thicker in the rippled-bed case than in the flat-bed case. Finally, near the lower limit of the profiles, the difference in the phase behavior of the stresses in the rippled- and flat-bed cases is particularly noticeable. This behavior is accounted for later by use of a convective eddy viscosity. It is important to point out that the velocity profiles in Figure 3a and the stresses in Figure 3b are well behaved and coherent in space and time. Hence, even though this might seem rather surprising, there is some a priori reason to attempt to relate the velocity gradients to the shear stresses via an eddy viscosity in the rippled-bed case.

[13] By the nature of the CIC model, the comparison depicted in Figure 3 ignores the Reynolds-stress contribution, $-\langle (u'v')_p \rangle$, to the convective stress, $\langle \tau_c \rangle$. While the model produces a Reynolds-stress-like contribution as a result of variability from cycle to cycle, this does not represent the physically based turbulent Reynolds stress. However, in practice, the Reynolds-stress contribution to $\langle \tau_c \rangle$ is a small one, as found by *Sleath* [1987] experimentally and by *Perrier et al.* [1995] using a Reynolds-stress, turbulence-closure model, which includes the contribution. Hereafter, in the discussion of the CIC model results, the Reynolds-stress contribution is neglected and the convective stress will be written simply as $-\langle uv \rangle$.

3.2. Calculating the Convective Eddy Viscosity Using Ranasoma's Measurements

[14] In this section the method of calculation of the mean and second harmonic of the eddy viscosity is outlined following the approach of *Davies and Villaret* [1997], and also the specific case of *Ranasoma*'s [1992] test 2a, used in that study, is reconstructed. This serves as a useful means of

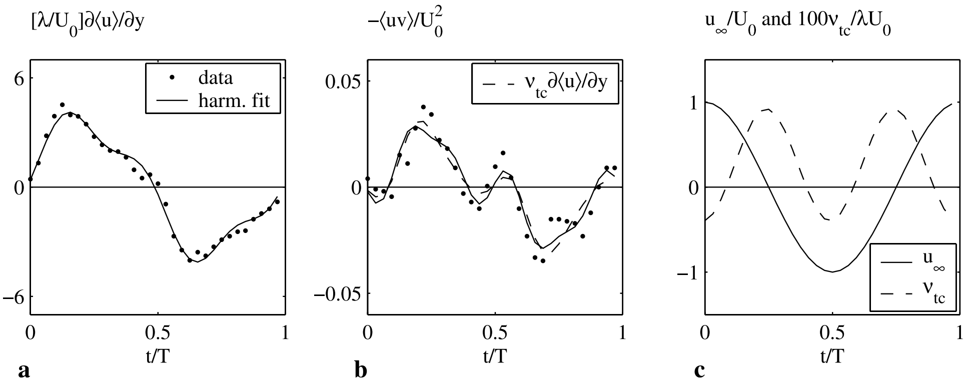

Figure 4. Illustration of the convective eddy viscosity approach in comparison with the data from *Ranasoma*'s [1992] test 2a at a height of $(y - \eta)/\lambda = 0.04$. Time series of the nondimensional (a) $\partial\langle u\rangle/\partial y$ with an harmonic fit using equation (7), (b) $-\langle uv\rangle$ with an harmonic fit using equation (6) and $\nu_{tc}\partial\langle u\rangle/\partial y$, and (c) free-stream velocity and convective eddy viscosity from equation (8).

illustration and also allows comparison with this earlier work when analyzing the present CIC model results. *Ranasoma* [1992] used Laser Doppler Anemometry to measure the velocity at 10 points in the horizontal and 4 points in the vertical above a fixed ripple in sinusoidally oscillating flow. The experimental conditions of test 2a were as follows: $T = 2.41$s, $\lambda = 10$ cm, $\eta/\lambda = 0.184$ and $A_0/\lambda = 0.78$. The (fixed) ripple shape was round-crested as shown in Figure 2.

[15] For symmetric wave oscillations, *Davies and Villaret* [1997] represented the convective shear stress and horizontally averaged velocity shear as power series of odd harmonics up to the fifth and third harmonics, respectively, and the convective eddy viscosity, ν_{tc}, as a mean and second harmonic,

$$-\langle uv\rangle = \mathrm{Re}\{\mathrm{T}_1\ \mathrm{e}^{i\sigma t} + \mathrm{T}_3\ \mathrm{e}^{i3\sigma t} + \mathrm{T}_5\ \mathrm{e}^{i5\sigma t} + \ldots\}, \tag{6}$$

$$\frac{\partial\langle u\rangle}{\partial y} = \mathrm{Re}\{S_1\ \mathrm{e}^{i\sigma t} + S_3\ \mathrm{e}^{i3\sigma t} + \ldots\}, \tag{7}$$

$$\nu_{tc} = \nu_{tc0} + \mathrm{Re}\{\nu_{tc2}\ \mathrm{e}^{i2\sigma t} + \ldots\}, \tag{8}$$

where $i = \sqrt{(-1)}$, Re denotes the real part, and the quantities are related by $-\langle uv\rangle = \nu_{tc}\partial\langle u\rangle/\partial y$. Using this definition and equations (6)–(8) and then equating coefficients of $\mathrm{e}^{i\sigma t}$, $\mathrm{e}^{i3\sigma t}$ and $\mathrm{e}^{i5\sigma t}$ results in

$$\mathrm{T}_1 = \nu_{tc0}S_1 + \frac{1}{2}\nu_{tc2}S_1^* + \frac{1}{2}\nu_{tc2}^*S_3, \tag{9}$$

$$\mathrm{T}_3 = \nu_{tc0}S_3 + \frac{1}{2}\nu_{tc2}S_1, \tag{10}$$

$$\mathrm{T}_5 = \frac{1}{2}\nu_{tc2}S_3, \tag{11}$$

where an asterisk denotes a complex conjugate. Since equations (9)–(11) are complex, they represent six equations in the three unknowns: ν_{tc0}, $\mathrm{Re}\{\nu_{tc2}\}$ and $\mathrm{Im}\{\nu_{tc2}\}$ (Im denotes the imaginary part). The unknowns in this overprescribed system of equations were estimated by *Davies and Villaret* [1997] using a least squares-fit method, and the same approach is adopted here.

[16] The behavior of the convective eddy viscosity is illustrated initially for the case of *Ranasoma*'s [1992] test 2a. The nature of the data, and the analysis of that data, have been discussed by *Davies and Villaret* [1997]. Figures 4a and 4b show the (nondimensional) horizontally averaged velocity shear and convective shear stress, respectively. In each case the solid line corresponds to the best harmonic fit involving the terms in equations (7) and (6). In Figure 4b the solid line for the shear stress has a substantial third harmonic component, which is not found in flat-bed cases such as that depicted in Figure 3d. An explanation for this convective shear stress behavior is given in the next section in terms of the vortex dynamics. The dashed line in Figure 4b corresponds to the reconstruction of the convective shear stress based on the product of the horizontally averaged velocity shear (solid line in Figure 4a) and the convective eddy viscosity (dashed line) shown in Figure 4c, obtained from the least squares procedure. Broad agreement is evident between the solid and dashed lines in Figure 4b. It can be seen in Figure 4c that the time variation in the eddy viscosity dominates over its mean value, and also that the eddy viscosity has its peak values at times of reversal in the free-stream flow (u_∞). This is consistent with the dominance of the vortex-shedding process above a rippled bed. It may be noted also that at times of maximum free-stream velocity, the eddy viscosity actually becomes negative. (For a discussion of negative eddy viscosity including some previous examples from the literature, see *Davies and Villaret* [1999].) In the present case, $\nu_{tc0}/\lambda U_0 = 0.0026$, $|\nu_{tc2}|/\nu_{tc0} = 2.5$ and $\arg(\nu_{tc2}) = 3.2$ ($\sim 180°$), as obtained previously by *Davies and Villaret* [1997]. The method used to calculate the mean and second harmonic of the convective eddy viscosity having been established, the present CIC model results are next analyzed in the same way and compared with Ranasoma's data.

3.3. Comparison Between CIC Model Results and Ranasoma's Data

[17] This comparison was first performed by *Perrier et al.* [1995] using a CIC model and, initially, their results are discussed in relation to those obtained from the present CIC model. This is a useful exercise since Ranasoma's data contained too few points in the vertical to allow a full model

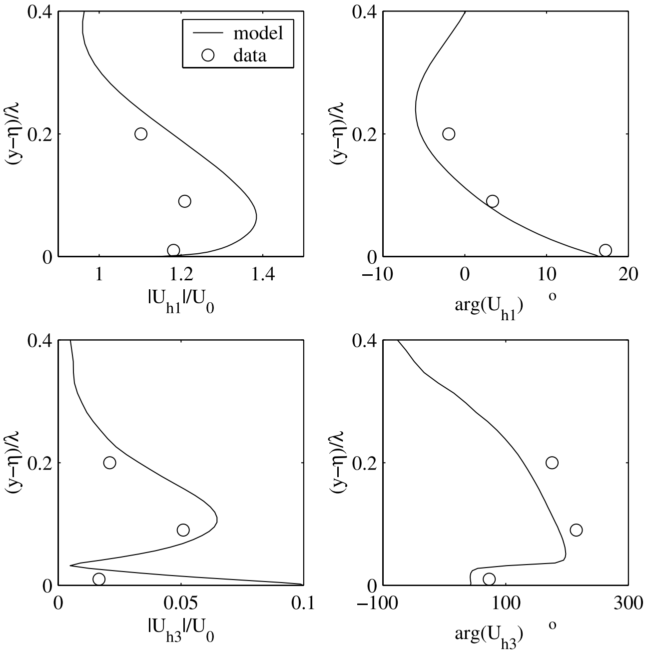

Figure 5. Vertical profiles of the first and third harmonics of horizontally averaged velocity (U_{h1} and U_{h3}) for *Ranasoma*'s [1992] test 2a from the present model and the data.

validation; an intercomparison of models allows at least some bounds to be put on the inferred convective eddy viscosity.

[18] The horizontally averaged velocity, $\langle u \rangle$, consistent with equation (7) may be written as

$$\langle u \rangle = \mathrm{Re}\{U_{h1}\ e^{i\sigma t} + U_{h3}\ e^{i3\sigma t} + \ldots\}. \tag{12}$$

In Figure 5, a comparison is made between the first and third harmonics of the horizontally averaged velocity for *Ranasoma*'s [1992] test 2a using a round-crested ripple shape (see Figure 2). The model agrees quite well with the data in terms of both amplitude and phase, though it seems to overpredict the overshoot of the amplitude of the first harmonic. The phase angle of the first harmonic is particularly well predicted, suggesting a lead of about 17° at the crest level, which decreases to zero at a height of 0.1λ above the crest. In the case of the third harmonic, the present CIC model captures the maximum in the amplitude away from the crest level (at a height of 0.1λ) and the associated phase behavior. Overall, the behavior of these harmonics is qualitatively similar to their flat-bed equivalents [see *Trowbridge and Madsen*, 1984].

[19] In Figure 6, a comparison of time series of $-\langle uv \rangle$ at three different heights is made between the data and the present model. The comparison is for the positive wave half cycle ($-90° \leq \sigma t < 90°$). It can be seen that there is broad agreement in behavior between the model and the data, though the results differ quite significantly in magnitude. The reason for this discrepancy is unclear, since Perrier's CIC model produced values of $-\langle uv \rangle$ that were more closely comparable with the data. The slightly anomalous behavior of the present CIC model does seem to be peculiar to Ranasoma's settings, as seen later (Figure 9 in section 3.4) when the closely similar case of $A_0/\lambda = 0.8$ is discussed. The present model does produce the maximum and minimum at B and C. However, it appears that the first predicted minimum at A actually occurs in the data in the previous wave half cycle, though the data should be interpreted with some caution since $-\langle uv \rangle|_{-90°} \neq \langle uv \rangle|_{90°}$.

[20] The positions of the maxima and minima in the $-\langle uv \rangle$ time series were explained by *Perrier* [1996] in terms of "bursts" and "sweeps." The first minimum, A, occurs when the newly ejected vortex passes over its "parent" crest; the maximum, B, occurs as a result of the next growing vortex in the trough; and the second minimum, C, occurs because the negative effect of the ejected vortex being forced upward as it passes over a neighboring crest momentarily outweighs the continuing positive effect of the growing vortex (for vortex positions, see Figure 2). This sequence of events is necessarily particular to the value of A_0/λ in Ranasoma's test. The effect of the ejected and growing vortex on $-\langle uv \rangle$ is shown schematically in Figure 7 for a free-stream flow that is positive. This shows that when the vortex generated in the previous wave half cycle is ejected by the positive flow, and is subsequently forced over neighboring crests, the "crest constriction" of the flow together with the vortex circulation means that faster moving fluid is circulated upward and slower moving fluid is circulated downward and therefore $-\langle uv \rangle < 0$ when $\langle u \rangle > 0$, as in the case of the minima at A and C in Figure 6b. On the other hand, the effect of the growing vortex results in a combined bursting and sweeping effect on the flow; slower moving fluid is circulated upward and faster moving fluid is circulated downward, giving $-\langle uv \rangle > 0$ when $\langle u \rangle > 0$, as in the case of the maximum at B in Figure 6b.

[21] Figures 8a and 8b show the eddy viscosity coefficients in equation (8) for Ranasoma's case (test 2a) inferred from the present CIC model. The overall structure of the two coefficients ν_{tc0} and ν_{tc2} is quite similar to that obtained

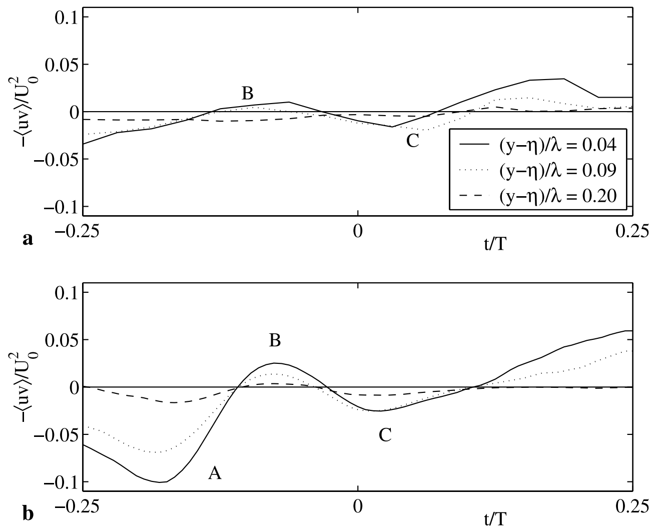

Figure 6. Time series of $-\langle uv \rangle$ for *Ranasoma*'s [1992] test 2a at different $(y - \eta)/\lambda$ for (a) the data and (b) the present model. The two minima and the maximum are labeled A, C, and B, respectively ($\eta/\lambda = 0.184$ and $A_0/\lambda = 0.78$).

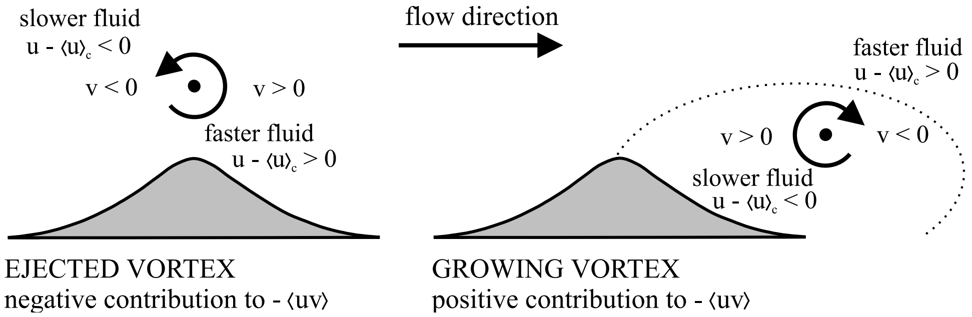

Figure 7. Sketch showing the ejected and growing vortex contribution to $-\langle uv \rangle$ based on an analogy with turbulent "bursts" and "sweeps" for positive free-stream flow where $\langle u \rangle_c$ is the horizontally averaged velocity through the center of the vortex.

by *Perrier et al.* [1995], but the magnitudes are rather different, as discussed later. Both ν_{tc0} and ν_{tc2} have their largest values in a layer of thickness equal to about 2 ripple heights above the mean bed level (i.e., up to $y - \eta = 1.5\eta$). Both terms exhibit a complicated vertical structure in this layer, with maxima at comparatively small distances ($\approx 0.5\eta$) above the crest. One crucial feature of the results is the phase of the second harmonic. This is centered around 180° in the lower part of the flow, as found in the *Ranasoma* [1992] data, indicating that peak values of eddy viscosity occur at around times of reversal in the free-stream flow. Immediately above the crest level, however, in a layer of thickness $0.03\lambda = 0.16\eta$, there is a sharp phase lag in the second harmonic of the eddy viscosity. Here the behavior of the eddy viscosity should be interpreted with some caution since it is also characterized by a strongly negative mean and a noisy second harmonic amplitude that are again peculiar to the Ranasoma settings. Above this, however, in the remainder of the vortex layer (0.16η up to about 1.5η), a fairly systematic phase lead develops, suggesting that momentum transfer in the upper part of the layer occurs slightly ahead of that in the middle and lower parts of the layer. This behavior is qualitatively quite different from that which would be expected above a flat bed.

[22] *Davies and Villaret* [1997] used the eddy viscosity interpreted from both *Ranasoma*'s [1992] data and also *Perrier et al.*'s [1995] CIC model results to confirm their simplified approach of assuming that in the near-bed layer, the eddy viscosity could be considered constant with height, with a second harmonic having a fixed magnitude and phase angle. Davies and Villaret took an average of the Perrier model results for the eddy viscosity in the height range $0.04 \leq (y - \eta)/\lambda \leq 0.2$, where $\arg(\nu_{tc2}) \approx 180°$, to quantify the mean and second harmonic of the eddy viscosity. A vertical average over a comparable height range, $0.03 \leq (y - \eta)/\lambda \leq 0.2$, was used for the results from the present model. These averages together with results obtained at the bottom of this convective layer from Ranasoma's data, at $(y - \eta)/\lambda = 0.04$, are given in Table 1. The vertical averages, over the heights where $\arg(\nu_{tc2}) \sim 180°$, of the mean and the second harmonic in the eddy viscosity are referred to hereafter as K_0 and K_2, to distinguish them from ν_{tc0} and ν_{tc2}, and the vertically averaged eddy viscosity, K, is thus given by $K_0 + \mathrm{Re}\{K_2 e^{i2\sigma t}\}$. It can be seen that while both models predict similar magnitudes and phase angles for the second harmonic, in reasonable agreement with the data (the magnitudes being about 1.4 times that of the data), Perrier's model produces a mean value that agrees more closely with the data than the present CIC model (1.7 times larger compared to 3 times larger than the data). As shown later, however, the value of $|K_2|/K_0 = 1.1$ in Table 1 is atypical when compared with other results from the present model. For example, the values of ν_{tc0} and ν_{tc2}, for a sharp-crested ripple with $A_0/\lambda = 0.8$ and $\eta/\lambda = 0.16$ (see Figures 8c and 8d, where $\arg(\nu_{tc2}) \approx 180°$ when $0.01 \leq (y - \eta)/\lambda) \leq 0.15$), which are roughly comparable with Ranasoma's settings, result in $K_0/\lambda U_0 = 0.0040$ and $|K_2|/K_0 = 1.6$. These values are more in keeping with the other values in Table 1. The reason for the anomalous behavior of the present model in this particular case remains unclear. However, it is likely that the contrasting vertical scaling of the convective layer in Figures 8a and 8b and Figures 8c and 8d probably relates to the different ripple shapes considered, since *Perrier et al.* [1995] also found

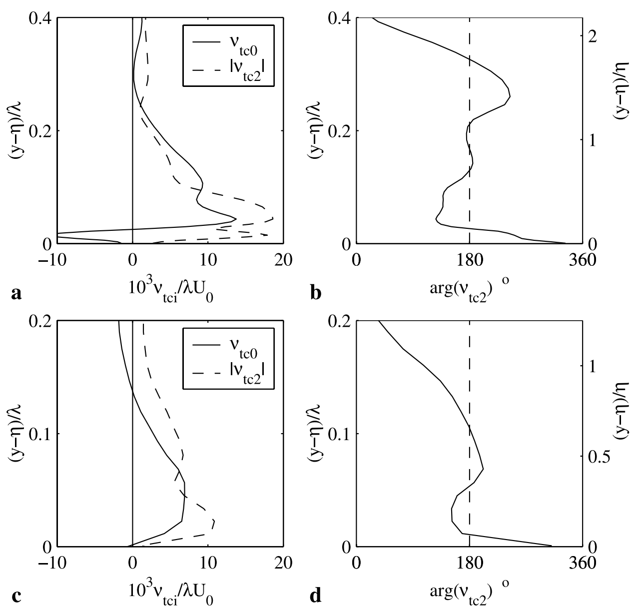

Figure 8. Profiles of the mean and second harmonic of the convective eddy viscosity above the crest level from the present model: (a, b) for *Ranasoma*'s [1992] test 2a (a round-crested ripple with $\eta/\lambda = 0.184$, $A_0/\lambda = 0.78$), and (c, d) for a sharp-crested ripple with $\eta/\lambda = 0.16$, $A_0/\lambda = 0.8$.

Table 1. Values of K_0 and $|K_2|$ Derived From the Data, *Perrier et al.*'s [1995] CIC model, and the Present CIC Model, for *Ranasoma*'s [1992] Test 2a

Origin	$K_0/\lambda U_0$	$\lvert K_2\rvert/\lambda U_0$	$\lvert K_2\rvert/K_0$	$\arg(K_2)$, Radians
Data	0.0026	0.0065	2.5	3.1
Perrier model	0.0043	0.0095	2.2	2.7
Present model	0.0082	0.0090	1.1	2.9

similar vertical scaling to that shown in Figures 8a and 8b. It should be stressed also that the values in Table 1 for the data are based on only one level and that the profiles of ν_{tc0} and ν_{tc2} from both CIC models, over the vortex-shedding height range, show rapid changes with height. Above the vortex-shedding range the magnitudes of ν_{tc0} and $|\nu_{tc2}|$ are much smaller (in Figure 8c, ν_{tc0} actually becomes negative). This reflects the fact that random turbulence (not included in the model) becomes increasingly important with height, and the neglect of the $-\langle(u'v')_p\rangle$ term in $\langle\tau_c\rangle$ can probably no longer be justified. The convective eddy viscosity from the present model having been tested against available data and a previous CIC model, its dependence on other parameters is considered in the next section.

3.4. Dependence of the Convective Eddy Viscosity on A_0/λ and η/λ

[23] In this section the dependence of the eddy viscosity on A_0/λ and η/λ, as characterized by the height-averaged values K_0 and K_2, is investigated. However, it is instructive to first examine the nature of the horizontal averages used to determine K_0 and K_2. For this purpose, attention is focused on sharp-crested ripples (see equation (1)) having wavelength λ = 22 cm, and waves having period T = 8.46 s, including η/λ = 0.16 and A_0/λ = 0.8, 1.2, and 1.8. These settings correspond to the experimental conditions of *Earnshaw* [1996] that were the subject of an earlier comparison with the present model [see *Malarkey and Davies*, 2002].

[24] Though the behavior of $\langle u\rangle$ is broadly similar to that depicted in Figure 5 as the value of A_0/λ is varied, pronounced changes occur in the time series of $-\langle uv\rangle$. In Figure 9 it can be seen that, for A_0/λ = 0.8, the time series of $-\langle uv\rangle$ is much the same as that shown in Figure 6b though, interestingly, the position of the first maximum appears to be closer to that seen in Ranasoma's data (Figure 6a). However, as A_0/λ increases, while the basic structure of $-\langle uv\rangle$ remains the same, it is apparent that more and more secondary maxima and minima occur. This is because larger values of A_0/λ result in more instances where ejected vortices are forced over successive ripple crests. As a result of this, higher harmonics in $-\langle uv\rangle$ become more important as A_0/λ increases. However, no corresponding higher harmonics are apparent in $\partial\langle u\rangle/\partial y$; in fact, the time series of $\partial\langle u\rangle/\partial y$ continue to look much the same as in Figure 4a. This means that the procedure outlined in section 3.2 to calculate ν_{tc0} and ν_{tc2} remains valid even though the first harmonic in $-\langle uv\rangle$, namely T_1, becomes weaker as A_0/λ increases. It should also be emphasized that using only a mean and a second harmonic to describe the eddy viscosity, while not representing the eddy viscosity fully, nevertheless gives a lowest order approximation to its time variation.

[25] For very rough beds, when vortex shedding is expected to be the dominant process, *Sleath* [1991] and also *Nielsen* [1992] proposed that the eddy viscosity could be considered constant in both height and time. They used similar data sets to derive the following expressions:

Sleath [1991]

$$\frac{K_0}{A_0 U_0} = 0.00253\sqrt{\frac{k_s}{A_0}}, \quad 1 \leq A_0/k_s \leq 120, \qquad (13)$$

Nielsen [1992]

$$\frac{K_0}{A_0 U_0} = 0.004\frac{k_s}{A_0}, \quad A_0/k_s \leq 16, \qquad (14)$$

where k_s is the equivalent bed roughness. These formulae, equations (13) and (14), have different dependencies because Sleath used turbulence measurements above the convective layer and Nielsen used measurements of the phase-ensembled, horizontal defect velocity, both within and above the convective layer, to represent the boundary layer as a whole. However, *Davies and Villaret* [1997] pointed out that in the rippled-bed regime $1 \leq A_0/k_s \leq 4$, equations (13) and (14) give similar results and, at A_0/k_s = 2.5, they give identical results. If it is assumed that $k_s = 4\eta$ [*Fredsøe et al.*, 1999], equations (13) and (14) can be expressed in terms of A_0/λ and η/λ as follows:

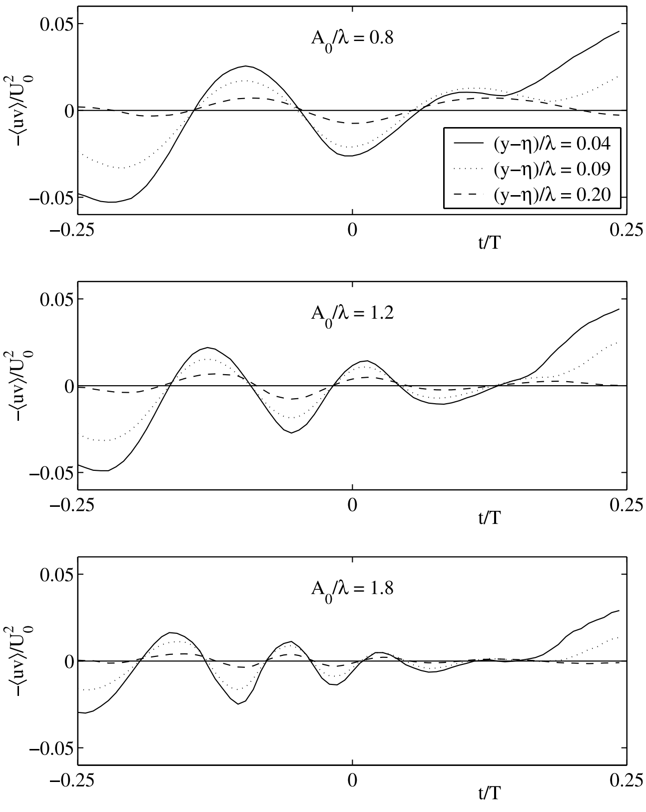

Figure 9. Time series of $-\langle uv\rangle$ for various A_0/λ for a sharp-crested ripple with η/λ = 0.16. The results correspond to the same nondimensional heights as in Figure 6.

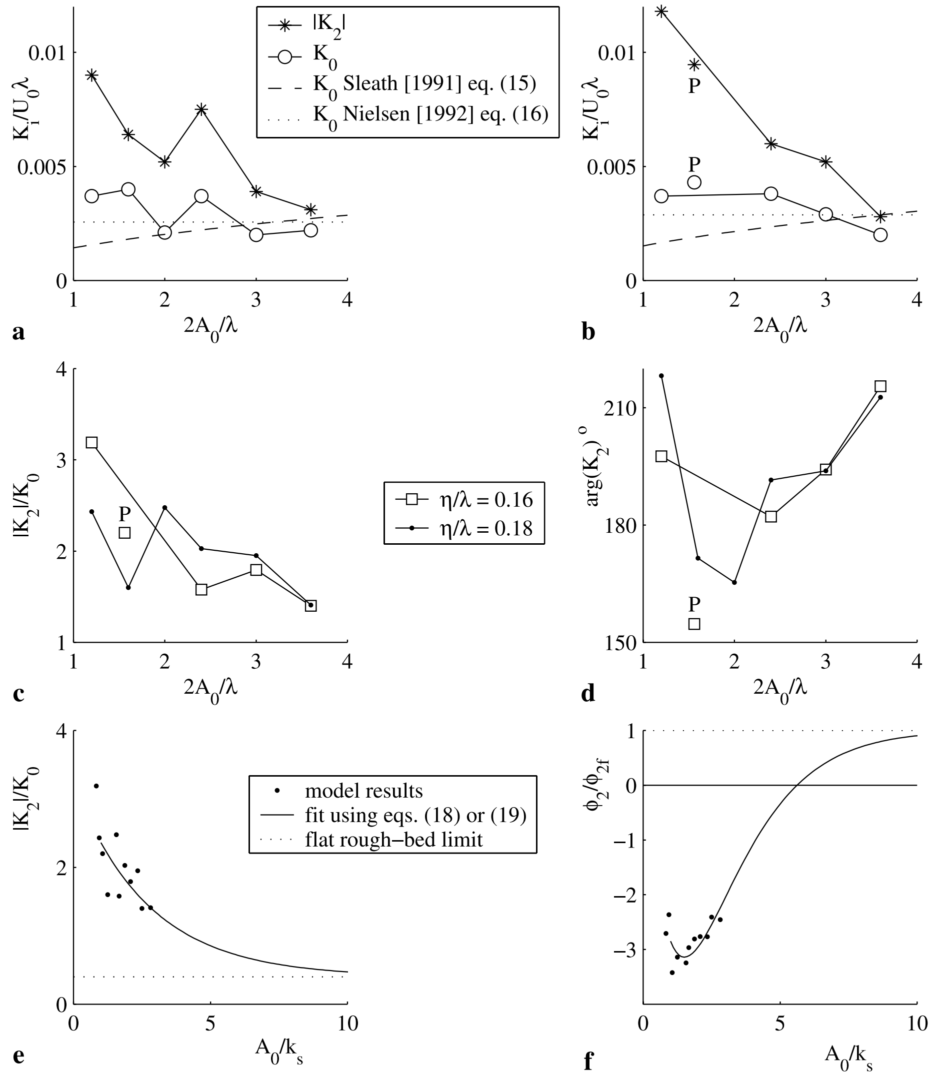

Figure 10. Nondimensional convective eddy viscosity for sharp-crested ripples versus A_0/λ, for (a) $\eta/\lambda = 0.16$ and (b) $\eta/\lambda = 0.18$. (c) $|K_2|/K_0$ and (d) $\arg(K_2)$ versus A_0/λ, for both steepnesses, from the present model. In Figures 10b, 10c, and 10d the symbols marked with P correspond to the values of Perrier from Table 1. (e) $|K_2|/K_0$ versus A_0/k_s, where the flat rough-bed limit is 0.4, and (f) ϕ_2/ϕ_{2f} versus A_0/k_s, where $\phi_2 = \arg(K_2) - 360°$ and $\phi_{2f} = 60°$.

Sleath [1991]

$$\frac{K_0}{\lambda U_0} = 0.00506\sqrt{\frac{\eta A_0}{\lambda^2}}, \qquad (15)$$

Nielsen [1992]

$$\frac{K_0}{\lambda U_0} = 0.016\frac{\eta}{\lambda}. \qquad (16)$$

Davies and Villaret [1997] compared these formulae with the mean component of eddy viscosity obtained from Ranasoma's data. They concluded that the mean component of eddy viscosity using the convective approach was "in broad agreement with" that predicted by equations (15) and (16), but was in "rather closer agreement with" *Nielsen*'s [1992] equation (16), as expected since *Nielsen*'s [1992] equation was restricted to rougher beds. Here, for representative values of A_0/λ and η/λ, values of K_0 based on the present model solution are compared with these formulae. The dependence of the second harmonic in the eddy viscosity (K_2) on the same parameters is also considered, though here there are no experimental values for comparison other than those calculated for Ranasoma's data by *Davies and Villaret* [1997]. The eddy viscosity has been calculated in the same way as described in sections 3.2 and 3.3. In each case the vertical averaging of ν_{tc0} and $|\nu_{tc2}|$ is restricted to the height range where $\arg(\nu_{tc2}) \sim 180°$. This region is quite distinct and corresponds typically to $\eta < y \leq 2\eta$ (i.e., a layer of thickness of η above the ripple crest). Even though $\arg(\nu_{tc2})$ is close to 180°, it is not exactly equal to 180° and so a representative value of $\arg(K_2)$ has also been obtained over the same height range.

[26] Figures 10a and 10b show the dependence of K_0 and $|K_2|$ on A_0/λ for two different sharp-crested ripple steepnesses (η/λ = 0.16 and 0.18). It can be seen that

Perrier et al.'s [1995] results for the eddy viscosity from Table 1, which are included in Figure 10b, are in good agreement with those from the present model, despite the fact that Perrier's results were obtained for a different ripple shape. This agreement suggests that the distinction of ripple shape associated with vertical scaling (see Figure 8) is removed by the vertical averaging process. For both ripple steepnesses the mean eddy viscosity shows quite good agreement with *Sleath*'s [1991] equation (15), but even better agreement with *Nielsen*'s [1992] equation (16), as found by *Davies and Villaret* [1997], and thus the latter can be considered a suitable predictor for the mean value K_0.

[27] The behavior of the second harmonic, in Figures 10a and 10b, is quite similar for both ripple steepnesses: $|K_2|$ tends to decrease with increasing A_0/λ, thus following the behavior expected from Figure 9 based on the relative size of the first harmonic of the shear stress. In Figure 10c, the ratio $|K_2|/K_0$ for the two different steepnesses shows little consistent difference as A_0/λ is varied, and the value of Perrier agrees quite well with the general trend for the present model. For most values of A_0/λ, $|K_2|/K_0$ tends to be larger than the value of 1.3 used by *Davies and Villaret* [1997]. However, even this value, which was limited by the analytical nature of their solution, is significantly larger than typical values used for flat beds ($A_0/k_s \geq 30$). (For example, *Trowbridge and Madsen* [1984] obtained $|K_2|/K_0 = 0.4$ from a truncated Fourier series based on $K \propto |\tau_{xyb}/\rho|^{1/2}$ where τ_{xyb} is the bed shear stress, $\tau_{xyb}/\rho \propto \cos(\omega t + \gamma)$ and γ is the phase lead of the bed shear stress over the free-stream velocity.) Figure 10d shows that the phase of K_2 behaves similarly for the two different steepnesses as A_0/λ varies; there is a minimum in the middle of the range, and the phase angle tends to increase on either side of this point. The value of Perrier, also included in Figure 10d, is in keeping with this general trend. Since a phase angle of 180° corresponds to flow reversal, a phase of greater than 180° is ahead of flow reversal. Thus the vortices are, for the most part, being shed ahead of flow reversal in the present model solution. All of the phase angles plotted in Figure 10d are very different from typical values based on eddy viscosity formulations for flat beds which yield values of about 60°. Such values occur, in the flat-bed case, since the maximum eddy viscosity coincides with maximum stress in the wave cycle (see the explanation above for $|K_2|/K_0 = 0.4$). Since γ is the phase lead of the bed shear stress over the free-stream velocity, it can be expressed in terms of the phase angle of the maximum value of K_2 in the wave cycle, as follows:

$$\gamma = \frac{1}{2}\arg(K_2), \qquad (17)$$

and since $\gamma \approx 30°$ in the flat-bed case (see, for example, test 2 of *Jonsson and Carlsen* [1976], where $A_0/k_s = 28.4$ for a fixed rough bed), it follows that $\arg(K_2) \approx 60°$. Both the phase angle and magnitude of the second harmonic in the eddy viscosity above a rippled bed, while being different from their flat-bed counterparts, nonetheless tend toward them as A_0/λ increases, since this corresponds to the bed becoming flatter (in the case of the phase angle this can be seen by considering the variation in $\arg(K_2) - 360°$). Physically, this type of behavior has been explained by *Malarkey and Davies* [2002] as the decay of coherent vorticity into more random turbulence as vortices pass over successively more ripples as A_0/λ increases.

[28] Model results for oscillatory boundary layer flow above flat beds in the rough turbulent regime are normally interpreted in terms of the parameter A_0/k_s. Thus it is of interest to quantify the behavior seen in Figure 10c in terms of A_0/k_s. Since $|K_2|/K_0$ should tend to its flat-bed limit of 0.4, as A_0/k_s becomes large, it seems reasonable to fit the following type of variation:

$$\frac{|K_2|}{K_0} = 0.4 + \varsigma_1 \exp\left[-\varsigma_2 \frac{A_0}{k_s}\right], \quad A_0/k_s \geq 1. \qquad (18)$$

Using a least squares-fit technique of the model results to equation (18), including the value of Perrier, gives $\varsigma_1 = 2.8$ and $\varsigma_2 = 0.36$. This best fit is shown in Figure 10e. Equation (18) predicts that $|K_2|/K_0$ is within 1% of its flat-bed value (= 0.4) when $A_0/k_s \approx 18$. Although a rather smooth variation in A_0/k_s has been assumed, the final outcome is reasonably consistent with the flat-bed limit being achieved at $A_0/k_s = 30$. As A_0/k_s increases and $|K_2|/K_0$ decreases, the phase intervals during the cycle when K becomes negative decrease and, for $A_0/k_s \geq 4.3$, they disappear. Implementation of the present rule (equation (18)) within a numerical model requiring non-negative values of the eddy viscosity at all phase angles is evidently not possible for $A_0/k_s < 4.3$. Here a pragmatic approach might be required whereby, for example, the mean eddy viscosity is increased to the value $(K_0 + |K_2|)/2$, and the magnitude of second harmonic is equated to this, such that the eddy viscosity does not become negative, and retains its original maximum value of $K_0 + |K_2|$. While such an adjustment is ad hoc, it maintains the spirit of the approach proposed here.

[29] A similar process can be used for the phase of K_2, namely $\phi_2 = \arg(K_2) - 360°$, under the constraint that it reverts to its flat-bed limit, $\phi_{2f} = 60°$, at large A_0/k_s. Here the following expression has been used:

$$\frac{\phi_2}{\phi_{2f}} = 1 - \varsigma_3 \frac{A_0}{k_s} \exp\left[-\varsigma_4 \frac{A_0}{k_s}\right], \quad A_0/k_s \geq 1. \qquad (19)$$

The critical phase angle of 180° identified in Figure 8b corresponds to $\phi_2/\phi_{2f} = -3$. Again using a least squares-fit technique on the model results to equation (19), with Perrier's value included, gives $\varsigma_3 = 7.5$ and $\varsigma_4 = 0.67$. The best fit curve, shown in Figure 10f, predicts that ϕ_2 is within 1% of its flat-bed value (= 60°) when $A_0/k_s \approx 14$, which is comparable with the value found for $|K_2|/K_0$ above. Also, it can be seen that $\phi = 0°$ when $A_0/k_s = 5.6$; in other words the eddy viscosity and shear stress are in phase with the free-stream flow. (This must occur since the shear stress lags behind the free-stream velocity in the rippled-bed case (see, for example, Figure 4b), and the shear stress leads the free-stream velocity in the flat rough-bed case.) Although the least squares-fitting techniques described above involve a large amount of extrapolation, the resulting decay rates are nonetheless consistent with one another. These two results, equations (18) and (19), together with equation (14), provide potentially useful rules for "connecting" the rippled-bed regime to the flat rough-bed regime in "very rough" to "rough" turbulent oscillatory flow.

[30] To demonstrate the harmonic method used in this paper, and to test the equations representing a height-

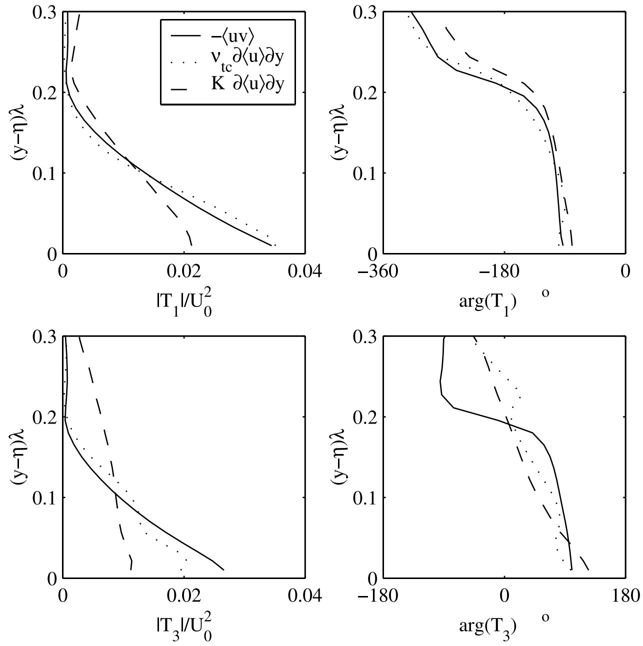

Figure 11. Vertical profiles of the first and third harmonics of convective stress from $-\langle uv\rangle$ and using the height-varying and height-invariant eddy viscosities, ν_{tc} and K, respectively, for a sharp-crested ripple with A_0/λ = 1.2 and η/λ = 0.18.

invariant eddy viscosity in the rippled-bed regime, the harmonics of the stress are reconstructed for a particular case. The first and third harmonics of the stress can be calculated by substituting the eddy viscosity coefficients, ν_{tc0} and ν_{tc2}, and vertical shear harmonics, S_1 and S_3, into equations (9) and (10). These stress harmonics can then be compared with the harmonics calculated directly from $-\langle uv\rangle$. This comparison is shown in Figure 11 for the case of A_0/λ = 1.2 and η/λ = 0.18, as depicted in Figure 10b. It is clear from this comparison that the harmonic reconstruction using the height-dependent eddy viscosity reproduces the harmonics calculated from $-\langle uv\rangle$ very well, thus validating the method used herein. Also shown in Figure 11 are the harmonics of stress again using equations (9) and (10) but with $\nu_{tc0} = K_0$ and $\nu_{tc2} = K_2$, where K_0 and K_2 are given by equations (14), (18), and (19). It can be seen that this height-invariant eddy viscosity produces the amplitudes and phases of the two harmonics reasonably well, but tends to under-predict the amplitudes near the crest and overpredict them farther away from the crest.

4. Discussion

[31] Since the purpose of the present work has been to represent the vortex-shedding process above ripples in a 1DV framework, it is necessary to consider whether the convective eddy viscosity characterized by equations (14), (18) and (19) can reasonably be implemented in a 1DV model. *Davies and Thorne* [2002] used a convective eddy viscosity, in a near-bed submodel, that had its mean value set by *Nielsen*'s [1992] equation (14). This has been confirmed by the results in the present paper. However, the second harmonic used by *Davies and Thorne* [2002] was limited by the size of the mean, because the eddy viscosity is restricted to positive values in most numerical models, as discussed earlier. Since the results here suggest that the second harmonic should be greater than the mean in the vortex-shedding layer, there is perhaps a need for an analytical solution involving a second harmonic with a relative magnitude that decreases with height. This solution could be used in an extended analytical approach, for example, in a transitional region above the present vortex-shedding region, such that, at the top of the transitional layer, where the analytical and numerical models are matched, the numerical constraint on the eddy viscosity is not broken. Certainly the assumption of a height invariant eddy viscosity seems rather crude in the light of the present model results (see Figure 8). It is also likely that the turbulent contribution to the eddy viscosity, resulting from the $-\langle (u'v')_p\rangle$ term in the stress, which is neglected in the present calculations, becomes increasingly important with height above the ripple. On the other hand, by assuming a height-invariant eddy viscosity, the effect of turbulence may be being included in the outer part of the boundary layer, but probably too much is being removed from the inner part, as demonstrated in Figure 11.

[32] At the edge of their vortex layer, *Davies and Thorne* [2002] prescribed the turbulent kinetic energy in terms of the eddy viscosity and a mixing length. This raises the more general question of how Reynolds-averaged quantities, such as the turbulent kinetic energy and the energy dissipation rate, behave in the convective layer. The behavior of such quantities in a one-dimensional framework can only be fully understood by analyzing horizontally averaged measurements or results from suitable two-dimensional, Reynolds-averaged models. Use of a two-dimensional Reynolds-averaged model would also allow the stress contribution $-\langle (u'v')_p\rangle$, referred to above, to be quantified and included in the earlier calculations.

[33] It should be pointed out also that while equations (18) and (19) provide a connection between the rippled- and flat-bed regimes, they are based only on matching the limiting cases. Thus they do not specify how, for example, the vertical structure of the eddy viscosity changes from constant to linearly increasing with height over the transitional range. The main transitional range $5 \le A_0/k_s \le 10$, where the flow field is changing from two- to three-dimensional is beyond the scope of not only the present CIC model, but any two-dimensional model, as pointed out by *Malarkey and Davies* [2002].

[34] In terms of future work, it would be interesting to quantify the increasing effect with height above the ripple crest of the horizontally averaged Reynolds-stress term. It would also be of interest to generalize the approach described in this paper to the asymmetric case, both for waves in isolation and also for waves combined with currents, by including a first harmonic in the eddy viscosity. This might help to verify the behavior of the eddy viscosity suggested by *Davies and Villaret* [1999] for weakly asymmetric progressive waves. Also, it might allow 1DV models to represent the enhanced current veering, resulting from asymmetric frictional drag in the two halves of the wave cycle when waves and currents are superimposed at some general angle over ripples, found by *Andersen and Faraci* [2003]. However, the most important next step should

be to analyze the horizontally averaged concentration in a two-dimensional model to see how the sediment concentration is affected by the corresponding "convective sediment diffusivity."

5. Conclusions

[35] Momentum transfer in the lower part of the oscillating boundary layer above steep ripples is dominated by the process of vortex formation and shedding. This coherent two-dimensional (or three-dimensional) motion gives way in the upper part of the boundary layer to random turbulent motion. The resulting total boundary layer thickness is considerably larger than that found in oscillatory flow above flat beds. The aim of the present study has been to further develop a relatively simple, practical modeling approach that captures the essential physics of the vortex-shedding process.

[36] The "convective eddy viscosity" approach of *Davies and Villaret* [1997] sought to represent the process of vortex shedding above ripples in a one-dimensional framework; in particular, the eddy viscosity related the horizontally averaged "convective" shear stress to the horizontally averaged velocity gradient. In the present paper, the results from a two-dimensional horizontal-vertical (2DHV), cloud-in-cell, discrete-vortex model have been horizontally averaged and then used to investigate this convective eddy viscosity approach over a range of conditions characterizing the vortex-ripple regime.

[37] Analysis of the model results suggests that coherent motions exist in a "convective layer" of thickness corresponding to one to two ripple heights above the mean bed level, within which it is appropriate to use the convective eddy viscosity approach. Here the time mean value of the eddy viscosity has been found to agree well with the empirically derived formula of *Nielsen* [1992]. In addition, the time variation in the eddy viscosity has been found to be characterized by a strong second harmonic that decreases from about 3 times the mean value of the eddy viscosity to the size of the mean value, as the ratio of orbital excursion amplitude to ripple wavelength increases. Moreover, the second harmonic has a phase angle consistent with the maximum value of the eddy viscosity occurring at times of reversal in the free-stream flow. As the above ratio increases, the trend in both the phase angle and also the magnitude of the second harmonic has been found to be in keeping with the expected transition to values appropriate for a flat bed; these trends have been quantified here by predictive formulae suitable for use in more practical large-scale formulations. These new results should contribute ultimately to a better representation of sediment transport over rippled beds.

Notation

A_0 orbital excursion amplitude.
K $K_0 + \mathrm{Re}\{K_2 e^{i2\sigma t}\}$.
K_0 and K_2 ν_{tc0} and ν_{tc2} averaged over convective layer.
$\mathbf{R}$ Reynolds-stress term.
Re Reynolds number ($= U_0 A_0/\nu$).
S_1 and S_3 first and third harmonic amplitudes of $\partial\langle u\rangle/\partial y$.
T wave period.
U_0 free-stream velocity amplitude.
U_{h1} and U_{h3} first and third harmonic amplitudes of $\langle u\rangle$.
i $\sqrt{(-1)}$.
k_s bed roughness ($= 4\eta$).
p nonhydrostatic pressure.
t time.
u phase-ensembled horizontal velocity.
u' horizontal turbulent fluctuation.
$\langle u\rangle$ horizontally averaged horizontal velocity.
u_∞ free-stream velocity.
$-\langle (u'v')_p\rangle$ Reynolds stress contribution to $\langle\tau_c\rangle$.
$-\langle uv\rangle$ convective contribution to $\langle\tau_c\rangle$.
v phase-ensembled vertical velocity.
v' vertical turbulent fluctuation.
x horizontal coordinate.
$\hat{\mathbf{x}}$ horizontal unit vector.
y vertical coordinate.
$\hat{\mathbf{y}}$ vertical unit vector.
T_1, T_3, and T_5 first, third, and fifth harmonic amplitudes of $-\langle uv\rangle$.
γ phase lead of τ_{xyb} over u_∞.
η ripple height.
λ ripple wavelength.
ν kinematic viscosity.
ν_{tc} convective eddy viscosity.
ν_{tc0} and ν_{tc2} mean and second harmonic of ν_{tc}.
π 3.1415927.
ρ water density.
σ angular frequency of the wave ($= 2\pi/T$).
$\varsigma_1 - \varsigma_4$ fitting coefficients.
τ_{xx} Reynolds stress ($= -(u'^2)_p$).
τ_{xy} Reynolds stress ($= -(u'v')_p$).
τ_{yy} Reynolds stress ($= -v'^2)_p$).
τ_{xyb} bed shear stress over a flat bed.
$\langle\tau_c\rangle$ convective stress ($= -\langle (u'v')_p\rangle - \langle uv\rangle$).
ϕ_2 $\arg(K_2)$.
ϕ_{2f} $\arg(K_2)$ in the flat-bed limit ($= 60°$).
ω vorticity ($= \partial v/\partial x - \partial u/\partial y$).
∇ $\hat{\mathbf{x}}\partial/\partial x + \hat{\mathbf{y}}\partial/\partial y$.
$*$ denotes a complex conjugate e.g., S^*_2.
Re real part, for example, $\mathrm{Re}\{\nu_{tc2}\}$.
Im imaginary part, for example, $\mathrm{Im}\{\nu_{tc2}\}$.
$\langle\rangle$ horizontal average, for example, $\langle u\rangle$.
$()_p$ phase ensemble, for example, $(u'v')_p$.
arg() phase angle of a complex quantity $\arg(\nu_{tc2})$.
$||$ magnitude of a complex quantity $|\nu_{tc2}|$.

[38] **Acknowledgment.** This work was funded by the European Union partly under the MAST III SEDMOC project, MAS3-CT97-0115, and partly under the Fifth Framework SANDPIT project, EVK3-CT-2001-00056.

References

Andersen, K. H., and C. Faraci (2003), The wave plus current flow over vortex ripples at an arbitrary angle, *Coastal Eng.*, *47*(4), 431–441.
Chorin, A. J. (1973), Numerical study of slightly viscous flow, *J. Fluid Mech.*, *57*, 785–796.
Christiansen, J. P. (1973), Numerical simulation of hydrodynamics by the method of point vortices, *J. Comput. Phys.*, *13*, 363–379.
Davies, A. G., and P. D. Thorne (2002), 1DV-model of sand transport by waves and currents in the ripple bed regime, in *Proceedings of the 28th International Conference on Coastal Engineering*, pp. 2599–2611, World Sci., River Edge, N. J.

Davies, A. G., and C. Villaret (1997), Oscillatory flow over rippled beds: Boundary layer structure and wave-induced Eulerian drift, in *Gravity Waves in Water of Finite Depth, Advances in Fluid Mechanics*, edited by J. N. Hunt, pp. 215–254, Comput. Mech., Southampton, UK.

Davies, A. G., and C. Villaret (1999), Eulerian drift induced by progressive waves above rippled and very rough beds, *J. Geophys. Res.*, *104*(C1), 1465–1488.

Earnshaw, H. C. (1996), A study of flow over a rippled bed using particle image velocimetry, Ph.D. thesis, Univ. of Edinburgh, Edinburgh, UK.

Fredsøe, J., K. H. Andersen, and B. M. Sumer (1999), Wave plus current over a ripple-covered bed, *Coastal Eng.*, *38*(4), 177–221.

Jonsson, I. G., and N. A. Carlsen (1976), Experimental and theoretical investigations in an oscillatory turbulent boundary layer, *J. Hydraul. Res.*, *14*(1), 45–60.

Lewis, A. W., E. Hitching, G. Perrier, E. A. Hansen, H. C. Earnshaw, K. Eidsvik, C. Greated, B. M. Sumer, and A. Temperville (1995), Flow over vortex ripples: Models and experiments, paper presented at 2nd International Conference on Coastal Dynamics, Am. Soc. of Civ. Eng., Gdansk', Poland.

Longuet-Higgins, M. S. (1953), Mass transport in water waves, *Philos. Trans. R. Soc. London, Ser. A*, *245*, 535–581.

Malarkey, J. (2001), Modelling oscillatory flow over vortex ripples using the discrete vortex method, Ph.D. thesis, Univ. of Wales Bangor, Bangor, UK.

Malarkey, J., and A. G. Davies (2002), Discrete vortex modelling of oscillatory flow over ripples, *Appl. Ocean Res.*, *24*(3), 127–145.

Malarkey, J., A. G. Davies, and Z. Li (2003), A simple model of unsteady sheet flow sediment transport, *Coastal Eng.*, *48*(3), 171–188.

Nielsen, P. (1992), *Coastal Bottom Boundary Layers and Sediment Transport*, 324 pp., World Sci., River Edge, N. J.

Perrier, G. (1996), Numerical modelling of the transport of non-cohesive sediments by waves and current over a rippled bed, Ph.D. thesis, Orsay Univ., Paris.

Perrier, G., C. Villaret, A. G. Davies, and E. A. Hansen (1995), Numerical modelling of the oscillatory boundary layer over ripples, in *MAST G8-M Coastal Morphodynamics Project, Final Overall Meeting*, pp. 4.26–4.29, Delft Hydraul., Gdansk', Poland.

Ranasoma, K. I. M. (1992), Measurements in combined oscillatory and steady flow over rippled beds, Ph.D. thesis, Univ. of Cambridge, Cambridge, UK.

Ranasoma, K. I. M., and J. F. A. Sleath (1992), Velocity measurements close to rippled beds, paper presented at 23rd International Conference on Coastal Engineering, Am. Soc. of Civ. Eng., Venice, Italy.

Sarpkaya, T. (1989), Computational methods with vortices—The 1988 Freeman Scholar Lecture, *J. Fluids Eng.*, *111*, 5–52.

Sato, S., N. Mimura, and A. Watanabe (1984), Oscillatory boundary layer flow over rippled beds, paper presented at 19th International Conference on Coastal Engineering, Am. Soc. of Civ. Eng., Houston Tex.

Sleath, J. F. A. (1987), Turbulent oscillatory flow over rough beds, *J. Fluid Mech.*, *182*, 369–409.

Sleath, J. F. A. (1991), Velocities and shear stresses in wave-current flows, *J. Geophys. Res.*, *96*(C8), 15,237–15,244.

Trowbridge, J., and O. S. Madsen (1984), Turbulent wave boundary layers: 1. Model formulation and first-order solution, *J. Geophys. Res.*, *89*(C5), 7989–7997.

A. G. Davies and J. Malarkey, School of Ocean Sciences, University of Wales Bangor, Menai Bridge, Anglesey, LL59 5AB, UK. (a.g.davies@bangor.ac.uk; j.malarkey@bangor.ac.uk)